Biosensors and Bioelectronics 122 (2018) 43–50

Contents lists available at ScienceDirect

Biosensors and Bioelectronics

journal homepage: www.elsevier.com/locate/bios

A facile DNA strand displacement reaction sensing strategy of electrochemical biosensor based on N-carboxymethyl chitosan/molybdenum carbide nanocomposite for microRNA-21 detection

Liang Tian[a,b], Jinxu Qi[a], Xiangyu Ma[a], Xuejiao Wang[a], Chen Yao[a], Wei Song[a], Yihong Wang[a,*]

[a] School of Chemistry and Chemical Engineering, Southeast University, Nanjing 211189, PR China
[b] School of Environmental Science and Engineering, Hebei University of Science and Technology, Shijiazhuang, Hebei 050018, PR China

ARTICLE INFO

Keywords:
Electrochemical biosensor
Strand displacement reaction
N-Carboxymethyl chitosan/Mo_2C nanocomposite
MicroRNA-21

ABSTRACT

Herein, we report a facile enzyme-free microRNA (miRNA) target-triggered strand displacement reaction (SDR) amplification strategy with ferrocene (Fc) as a signal molecule to fabricate a two-dimensional electroactive molybdenum carbide (Mo_2C)-based biosensor. In the presence of miRNA-21, SDR was initiated and many hairpin DNA1 (HDNA1) and hairpin DNA2 (HDNA2) duplexes, which could be captured by probe DNA leading the Fc-modified HDNA2 close to the electrode surface, were produced continuously. MiRNA-21 could be detected by monitoring the redox signal of Fc. The prepared *N*-carboxymethyl chitosan/Mo_2C nanocomposite featured excellent conductivity, great dispersion, and multiple functional groups (amine groups). When the nanocomposite was introduced to a miRNA biosensor electrode interface to ensure its strong connection to the DNA probe, the developed miRNA-21 biosensor demonstrated a reliable linear range of 1.0 fM to 1.0 nM with a detection limit of 0.34 fM and showed good selectivity, reproducibility, and stability. The biosensor was employed to detect miRNA-21 in human serum samples, and it showed great potential in the early clinical diagnosis of various genetic diseases.

1. Introduction

MicroRNA (miRNA) are approximately 19–25 nucleotides long and regulate the control and development of cancer expression; as such, these molecules have received much attention as a biomarker (Dong et al., 2013). Early detection of miRNA is of great importance in the diagnosis, timely treatment, and recurrence prognosis of many diseases (Arya and Bhansali, 2011; Mak et al., 2016). Various detection technologies, such as northern blot analysis (Várallyay et al., 2008), real-time quantitative polymerase chain reaction (Yu et al., 2008), and microarray technology (Lee et al., 2010), have recently been developed to identify and quantify miRNA. However, these techniques present the disadvantages of prolonged assay times, high costs, large sample consumption, and complex operation, all of which limit their application in early diagnosis (Hou et al., 2015; Ullah et al., 2018). In addition, miRNA concentrations in peripheral blood plasma and serum often range from the femto- to nanomolar levels (Yang et al., 2018). As such, a highly sensitive detection method and signal enhancement strategy should be developed to address this limitation.

Electrochemical biosensors are a promising detection technique because of their relatively low cost, quick response, high sensitivity, good specificity, simple preparation, instrumentation accessibility, and application field scalability (Lisak et al., 2016; Tiwari et al., 2016; Wang et al., 2018a). Considering these features, electrochemical detection is more suitable for early diagnosis of cancer biomarkers than other analytical methods, such as surface plasmon resonance (Li et al., 2016c) and bioluminescence assay (Valenti et al., 2017), which have poor sensitivity and are time-consuming. To achieve high sensitivity, signal amplification strategies, such as exonuclease-assisted target recycling amplification (Sun et al., 2017), polymerase chain reaction (Nguyen et al., 2017), rolling circle amplification (RCA) (Feng et al., 2016), catalytic hairpin assembly (CHA) (Shi et al., 2017), hybridization chain reaction (HCR) (Yang et al., 2017; Ge et al., 2018), and strand displacement reaction (SDR) (Bi et al., 2016), are usually applied to biosensors. SDR shows great potential in signal amplification due to its unique merits (Yin et al., 2017; Yao et al., 2017; Hu et al., 2017; Li et al., 2016b), such as its capability of target-triggered cascade hybridization and displacement reactions between two hairpin DNAs and targets under mild conditions without the need for any natural enzyme. Moreover, SDR can significantly enhance electrochemical signals even when the target molecules exist only in trace amounts, and its amplification demonstrates high target selectivity. Compared with other non-

* Corresponding author.

https://doi.org/10.1016/j.bios.2018.09.037
Received 27 July 2018; Received in revised form 6 September 2018; Accepted 12 September 2018
Available online 13 September 2018
0956-5663/

enzyme circulation (e.g., CHA and HCR) methods, SDR possesses a relatively easier sequence design, which could reduce background signals (Chen et al., 2018) and carry the marked signal-amplification molecule close to the electrode surface to diminish the influence of mass transfer during the redox reaction; such a feature is suitable for electrochemical experiments (Jiang et al., 2018). Thus, in this work, we employed an SDR amplification strategy to improve the sensitivity of the miRNA electrochemical biosensor.

Two-dimensional (2D) materials have promoted rapid developments in the sensing field because of their intrinsic advantages. Many layered 2D nanosheets, such as graphene oxide (Azimzadeh et al., 2016), graphene (Sreekanth et al., 2016; Wang et al., 2018b), transition-metal dichalcogenides (MoS_2, WS_2) (Rohaizad et al., 2017), and transition-metal carbides (Xu et al., 2016), have been integrated into electrochemical biosensors. Although molybdenum carbide (Mo_2C) is considered a highly promising transition-metal carbide and has been applied in many fields, few studies exploring Mo_2C nanomaterials as functionalized units for the fabrication of electrochemical biosensors have been published (Zhai et al., 2016). Mo_2C is a representative transition-metal carbide due to its low cost, high surface area, excellent electrical conductivity, remarkable chemical stability, and strong mechanical strength. Various forms and phases of Mo_2C are used in many applications, including catalysis (Lin et al., 2018), immunosensing (Zhu et al., 2017), and as semiconductor (Halim et al., 2016). Mo_2C is commonly chosen as a supporting material on the electrode interface in electrochemical biosensors. However, large-scale preparation of 2D Mo_2C is usually affected by high-temperature sintering processes, resulting in the lack of functional groups in the final materials, which limits their further use. *N*-Carboxymethyl chitosan (NCS), a novel kind of chitosan (Cui et al., 2018), presents a number of excellent properties, including water solubility, rich functional groups (amine), film-formation ability, and biocompatibility, all of which could make great contributions to material modification and expand their applications. By coupling Mo_2C with NCS, the produced NCS/Mo_2C nano-complex, as a supporting electrode material, is expected to improve the sensitivity and stability of electrochemical biosensors. NCS/Mo_2C nano-complexes have an abundance of functional groups, which could be used to immobilize probe DNA (p-DNA) molecules or other biomolecules, and exhibit excellent dispersibility in aqueous solutions with high stability. Thus, a nanocomposite matrix film could be formed by drop casting an NCS/Mo_2C nano-complex onto the electrode to improve its stability and the sensitivity of the resulting biosensor.

In this paper, a novel electrochemical biosensor was developed for the detection of miRNA in standard and serum samples. An SDR strategy was applied to increase the signals of HDNA duplex molecules even when the target molecules exist only in trace amounts. An NCS/Mo_2C nano-complex, as a supporting electrode material, was used, for the first time, in the electrochemical biosensor-based detection of miRNA. The proposed biosensor displayed superior characteristics, such as high selectivity, low detection limit, and excellent recovery rates.

2. Experimental

2.1. Chemicals and reagents

Ammonium molybdate tetrahydrate, tris-(2-carboxyethyl)-phosphine-hydrochloride (TCEP) and the human serum samples (H4522) were purchased from Sigma-Aldrich, while N-(3-(dimethylaminopropyl)-N′-ethylcarbodiimide hydrochloride (EDC) and N-hydroxysuccinimide (NHS) were purchased from Aladdin Reagent Company (Shanghai, China). N-carboxymethyl chitosan was purchased from Zhejiang Golden-Shell Pharmaceutical Co., Ltd (Pharmaceutical Grade, MW: 2000–3000). All other reagents used were of analytical grade. In our work, 10 mM phosphate buffered saline (PBS pH 7.0) was used as supporting electrolyte. All aqueous solutions were prepared with ultrapure water (~18.2 MΩ cm) using an Aquapro water purification system. Chinese academy of sciences provided the cell lines (Hela and MCF-7). Oligonucleotides were obtained from Sangon Biotech Co., Ltd (Shanghai, China). The sequences of these oligonucleotides were shown in Table S1.

2.2. Apparatus and measurements

The electrochemical measurements were carried out using the CHI660E Electrochemical Workstation (Shanghai Chenhua Instrument Corporation, China) at room temperature. Measurement techniques include cyclic voltammetry (CV), electrochemical impedance spectroscopy (EIS), differential pulse voltammetry (DPV) and Amperometric i-t Curve (I-T). A conventional three electrode system which consists of a modified glassy carbon electrode (GCE, 3 mm in diameter, working electrode), a platinum wire (auxiliary electrode) and a saturated calomel electrode (SCE, reference electrode) was used in all electrochemical investigations, while EIS was performed in 5.0 mM $K_3Fe(CN)_6/K_4Fe(CN)_6$ mixture with 0.1 M KCl as supporting electrolyte, using an amplitude of 5 mV, within the frequency range of 0.1–10^5 Hz. Transmission electron microscopy (TEM) images were obtained from a FEI Tecnai G2 T20 microscope (USA). A digital pH-meter (780 pH meter, Metrohm) was used to read the pH value of the buffer solutions. Electrolyte solutions were deoxygenated by purging with pure nitrogen (99.99%) for 10 min prior to electrochemical experiments. All measurements were carried out under a nitrogen atmosphere.

2.3. Synthesis of Mo_2C nanosheets

2.3.1. Synthesis of NaCl templates

Synthesis of NaCl templates and Mo_2C nanosheet (Mo_2C NS) was performed according to the procedure reported by (Wu and Li, 2017) with slight modifications. First, NaCl powders were completely dissolved in deionized water to form a saturated solution. A large amount of ethanol was injected into the mixture under stirring, and a milky suspension was observed for the substantially decreased solubility. Finally, the obtained white NaCl crystals were collected, dried, and finely ground for further use.

2.3.2. Synthesis of Mo_2C NS

In a typical synthesis procedure, 50 mg of ammonium molybdate tetrahydrate and 50 mg of citric acid were dissolved in 1 mL of double-distilled water. Subsequently, 2 g of the NaCl templates was added into the solution, and the mixture was ultrasonicated for approximately 10 min. The obtained mixture was completely dried in an 80 °C oven overnight, and the obtained solid mixture was ground into very fine powder. After pyrolysis at 750 °C for 2 h with a ramp rate of 5 °C min^{-1} in an Ar atmosphere, the obtained product was repeatedly washed with distilled water to remove the NaCl templates under sonication and centrifugation. Finally, the black powders were collected and dried at 80 °C.

2.4. NCS modification of Mo_2C NS

Mo_2C NS was functionalized according to literature with some modifications (Dinshaw et al., 2017). Mo_2C NS was dispersed in water with ultrasonication for 30 min to obtain a homogenous suspension (1 mg mL^{-1}). A total of 1 mg mL^{-1} NCS solution was prepared by dissolving NCS powder in water with stirring for 1 h at room temperature until completely dissolution. Then, 5 mL of Mo_2C NS suspension (1 mg mL^{-1}) was added to 5 mL of the above NCS solution, and the mixture was ultrasonicated for 1 h. A black precipitate was collected by centrifugation and redispersed in deionized water. The resultant black suspension appeared homogeneous and stable.

2.5. Probe DNA immobilization of NCS/Mo_2C NS

Conjugation of NCS/Mo_2C NS with p-DNA was carried out with an EDC/sulfo NHS mixture solution (50 mg mL^{-1} each in MES buffer, pH 5.0) according to our previous report (Tian et al., 2018). The blocking step was accomplished with a 1 M ethanolamine solution prepared in 0.1 M phosphate buffer solution (pH 8.0), while EDC was equilibrated to room temperature. Then, 10 µL of 100 µM p-DNA was added to 200 µL of conjugation buffer. Thereafter, 2 mg of NCS/Mo_2C NS was dissolved in 500 µL of conjugation buffer, after which the solution was added to the previously prepared 200 µL of p-DNA in conjugation buffer. A separate solution of 10 mg of EDC in 1 mL of ultrapure water was prepared; 100 µL of this solution was immediately added to the p-DNA and NCS/Mo_2C NS solution, which was then allowed to react for 12 h at room temperature. The p-DNA/NCS/Mo_2C NS conjugate was purified using a centrifuge, redispersed in deionized water, and stored in a sterile container at 4 °C.

2.6. Fabrication of the target-triggered amplification biosensor

Prior to its use, a bare GCE was thoroughly polished with 1.0 and 0.05 µm alumina-water slurries on a smooth polishing cloth until a mirror-like surface was obtained. The GCE was then sonicated for 5 min in distilled deionized water to remove residual alumina particles, followed by thorough rinsing with distilled water and drying under a nitrogen flow. Then, 10 µL of p-DNA/NCS/Mo_2C NS composites was cast onto the electrode surface and dried at room temperature. HDNA1 and HDNA2 were heated to 95 °C for 5 min followed by cooling to room temperature for 2 h. The mixed solution was prepared by mixing 5 µL of 1 µM HDNA1, 5 µL of 1 µM HDNA2, and 5 µL of miRNA in different concentrations and incubating the same at 35 °C for 90 min. Finally, 15 µL of the above mixed solution was added to the p-DNA/NCS/Mo_2C NS modified GCE surface. After washing with PBS buffer to remove non-specific adsorption, the proposed miRNA biosensor was constructed as shown in Scheme 1.

2.7. MiRNA detection in cell extract

Cells were collected and rinsed with cold PBS (10 mM, pH 7.4) thrice and counted with a hemocytometer. Cells were cracked in lysis buffer to extract their miRNA. The supernatant was separated using centrifugation for 15 min at 10,000 × g under 4 °C.

3. Results and discussion

3.1. Design and possible mechanism of the electrochemical biosensor

The mechanism of the biosensor we proposed for sensitive detection of miRNA is detailed in Scheme 1. First, the prepared p-DNA/NCS/Mo_2C NS was modified on the GCE surface. In toehold mediated SDR process, HDNA1, HDNA2, and different concentration of target miRNA were mixed. When targeting exists, HDNA1 could first open the loop and hybrid with the target miRNA to form miRNA and HDNA1 duplexes. Subsequently, the target miRNA in the microRNA and HDNA1 duplexes could be substituted by the Fc-HDNA2 enzyme freely, releasing the target to open more HNDA1 for triggering many recyclic substituents. Many Fc-HDNA2 and HDNA1 duplexes were formed to enhance signal amplification. After dropping the remaining fragments of Fc-HDNA2&HDNA1 duplexes on the p-DNA/NCS/Mo2C NS/GCE, they can be captured by p-DNA. Fc redox molecules were carried close to the electrode surface to improve the electrochemical electronic transmission and mass transfer efficiency. Therefore, the amount of target miRNA can be evaluated through the electrochemical signal of Fc. In the absence of target miRNA, the loops of HDNA1 and HDNA2 could not be open, indicating that no SDR occurred and no Fc-HDNA2 and HDNA1 duplexes were formed, resulting in a weak electrochemical response as a control. Furthermore, DPV and I-T were carried out to verify electrochemical signal generation. As shown in Fig. 1A and B, the values of peak current and terminal current were small in the absence of target miRNA. However, after adding the target miRNA to trigger the SDR processes, Fc could undergo a redox reaction on the electrode and the amplified electrochemical signal was obtained. Thus, the currents were significantly enhanced and the values of curve b in Fig. 1A and B increased higher than the control. These results demonstrate that our strategy could improve the sensitivity of electrochemical detection for miRNA-21.

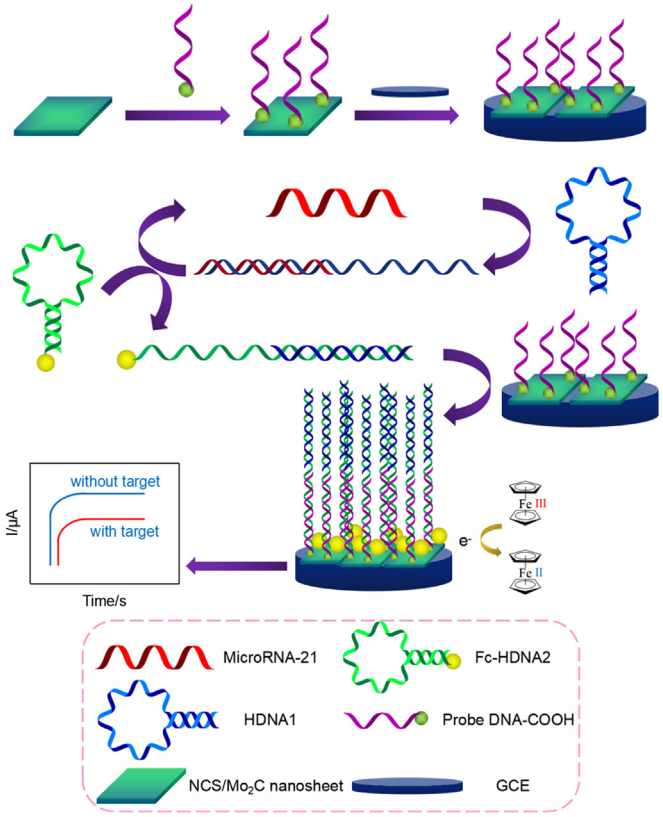

Scheme 1. Schematic illustration of NCS/Mo_2C NS based strand displacement reaction signal amplification for miRNA-21detection.

The cyclic voltammograms of the p-DNA/NCS/Mo_2C NS modified GCE were characterized at different scan rates, which could reflect the typical reversible electrochemical reaction (Fig. S1). The anodic and cathodic peak currents exhibited good linear proportion to the square root of the scan rate in the range of 10–200 mV/s from − 0.2–0.6 V. As shown in Fig. S1A, a pair of well-defined redox peaks appeared at different scan rates, and the redox peak currents were increased along with the increase of scan rates. A good linear relation was obtained between the redox peak current and the square root of the scan rate (Fig. S1B). The fine electrochemical behavior promises a diffusion-controlled redox process that can occur on the surface of the p-DNA/NCS/Mo_2C NS/GCE (Miao et al., 2016), which can be further used as ideal interface for the following experiments.

3.2. Characterization of the Mo_2C NS and NCS/Mo_2C NS

The morphologies of the as-synthesized nanomaterial were characterized using TEM. As shown in Fig. 2A, a large-scale thin layer of Mo_2C NS presented typical crumpled and wrinkled structures, thus suggesting that Mo_2C NS retains its 2D morphology and large surface area. The high-resolution TEM (HTEM) image of Mo_2C NS shown in Fig. 2B suggests that the Mo_2C NS is flexible, thin, and possibly few-layered or even mono-layered. The selected area electron diffraction

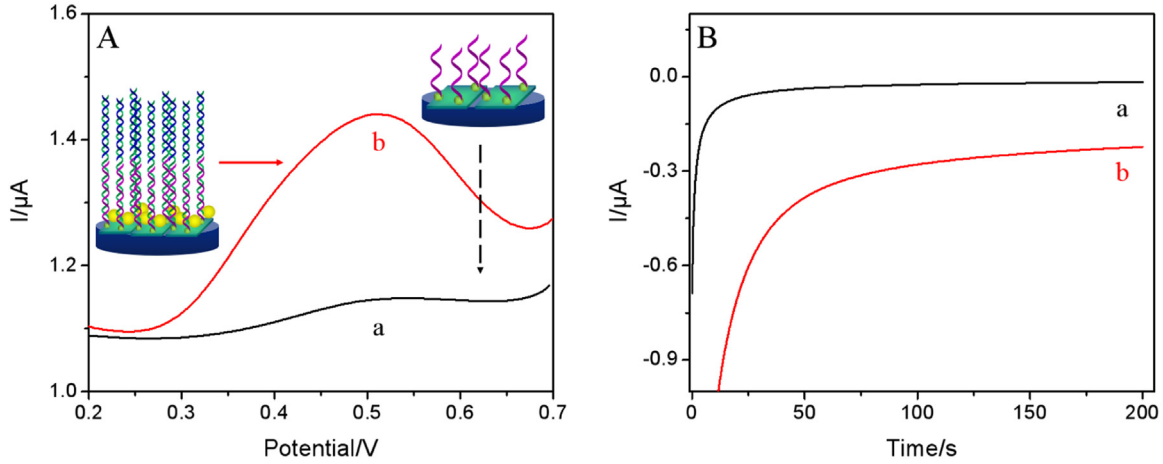

Fig. 1. DPV curves (A) and I–T curves (B) of p-DNA/NCS/Mo_2C NS/GCE before (a) and after (b) 1 nM miRNA-21 target-triggered SDR in 0.01 M PBS (pH = 7.0).

(SAED) pattern (inset in Fig. 2B) indicates that Mo_2C NS is well crystallized and displays a monocrystalline feature with hexagonal structure. After modification with NCS, the NCS/Mo_2C NS hybrid exhibited a smoother surface, as shown in Fig. 2D. The HTEM image of NCS/Mo_2C NS displays a thin layer possessing well-dispersed functional groups with NCS (Fig. 2E). The elemental compositions of Mo_2C NS and NCS/Mo_2C NS were further investigated using EDS. Compared with those in the EDS of Mo_2C NS (Fig. 2C), the N and O peaks in the elemental compositions of NCS/Mo_2C NS (Fig. 2F) indicated that the *N*-carboxymethyl chitosan/Mo_2C NS hybrid was successfully synthesized.

3.3. Characterization of biosensor fabrication

Cyclic voltammetry (CV) and electrochemical impedance spectroscopy (EIS) were used to verify the stepwise assembly processes of the modified electrodes. Fig. 3A illustrates typical cyclic voltammograms (CVs) of $K_3[Fe(CN)_6]/K_4[Fe(CN)_6]$ at different surface electrodes with several reversible redox peaks for the bare GCE (curve a). When NCS/Mo_2C NS was modified onto the electrode, the peak current of the electrode slightly decreased (curve b) due to the weak conductivity of NCS. However, Mo_2C NS on the electrode could increase the surface area and provide more active sites per unit area. Moreover, after

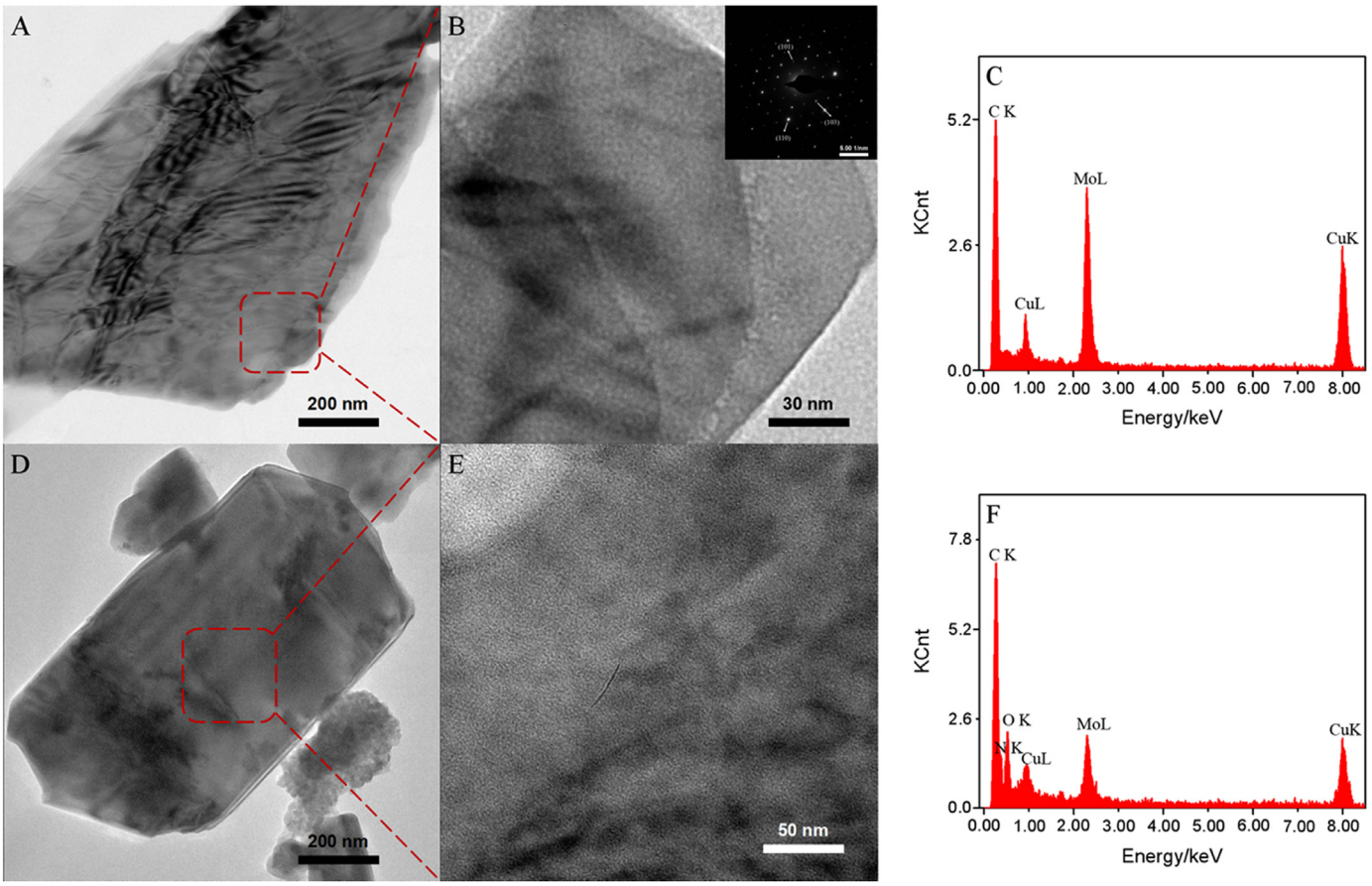

Fig. 2. TEM image of Mo_2C NS (A), HRTEM image of Mo_2C NS (B) with selected area electron diffraction (SAED) pattern (inset), and EDS spectrum of Mo_2C NS (C). TEM image of NCS/Mo_2C NS (D), HRTEM image of NCS/Mo_2C NS (E), and EDS spectrum of NCS/Mo_2C NS (F).

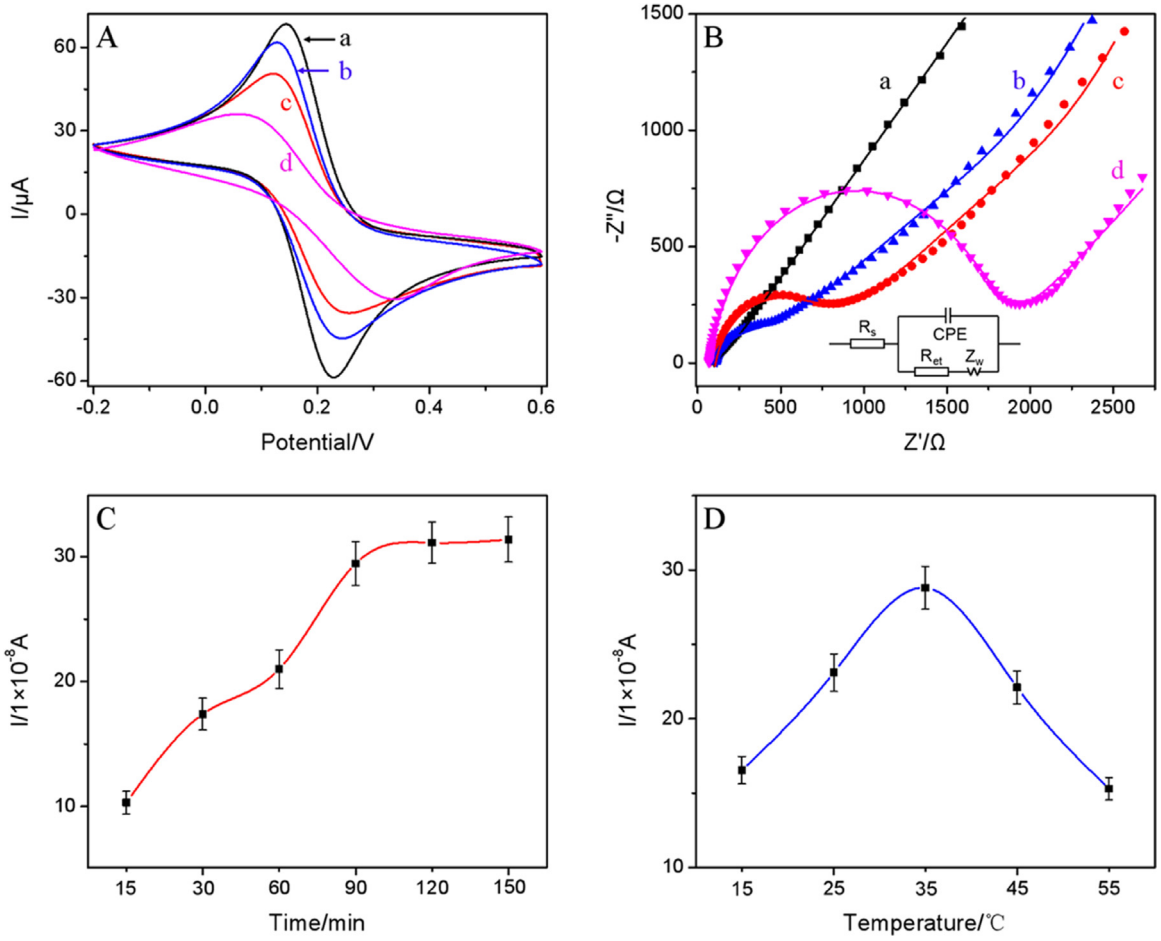

Fig. 3. (A) Cyclic voltammograms and (B) Nyquist plots of electrochemical impedance spectra of bare GCE (a), NCS/Mo_2C NS/GCE (b), p-DNA/NCS/Mo_2C NS/GCE (c) and HDNA2&HDNA1/p-DNA/NCS/Mo_2C NS/GCE (d) in 5.0 mmol L^{-1} $[Fe(CN)_6]^{3-/4-}$ containing 0.1 mol L^{-1} KCl at 100 mV/s, and the frequency range is at 100 mHz to 100 kHz with amplitude of 5 mV (The inset is the equivalent circuit of the Nyquist plots). Optimization of the experimental parameters: effects of incubation time (C) and incubation temperature (D) on HDNA1 and HDNA2 incubated within 1 nM miRNA-21 solution recorded by I-T in 0.01 M PBS (pH = 7.0). Error bars = RSD (n = 5).

immobilization of p-DNA, the current decreased due to the negatively charged oligonucleotides and spatial blockage of $[Fe(CN)_6]^{3-/4-}$ ions by oligo molecules to reach the electrode surface (curve c). After coating with HDNA1 and HDNA2, the charge transfer ability of these molecules decreased, resulting in a decreased current response (curve d). This observation indicates that the adherence of HDNA1 and HDNA2 effectively blocks charge and mass transfer between the redox couple in the solution and GCE electrode.

Fig. 3B shows the impedance spectra in the form of Nyquist plots of the interfaces recorded after each modification step. The spectra were analyzed using Zview2 software, which uses a nonlinear least-square fit to determine the parameters of the elements in the equivalent circuit, which consisted of solution resistance (Rs), electron transfer resistance (Ret), constant-phase element (CPE), and Warburg impedance (Zw), as shown in the Fig. 3B inset. Due to weak conductivity, NCS/Mo_2C NS modified GCE of 218.5 Ω (curve b) exhibited a higher Ret than the bare GCE of 78.53 Ω (curve a). Subsequently, when the modified electrode was hybridized with p-DNA (curve c), the diameter of the semicircular part successively increased with the Ret also increasing to 579.4 Ω. The binding of HDNA1 and HDNA2 further increased Ret to 1664 Ω (curve d), since hybridization of HDNA1 and HDNA2 on the electrode surface effectively blocked the charge transfer between the electrode surface and the electroactive probe, $[Fe(CN)_6]^{3-}/[Fe(CN)_6]^{4-}$, while it increased the impedance between the solution and the electrode. These results are consistent with the phenomena in CVs, which confirmed the successful preparation of the biosensor.

3.4. Optimization of experimental parameters

First, the incubation times of HDNA1, HDNA2, and the target molecule were investigated, as shown in Fig. 3C. The current increased as the incubation time increased from 15 min to 90 min and then plateaued when the incubation time was prolonged from 90 to 150 min. Therefore, 90 min was selected as the best incubation time of the target miRNA with HDNA1 and HDNA2. The effect of hybridization temperature was induced by incubating miRNA with HDNA1 and HDNA2 for 90 min at different temperatures ranging from 15 °C to 55 °C (Fig. 3D). Results showed that the peak current value increased as the hybridization temperature increased from 15 °C to 35 °C. This behavior depicts an increased extent of displacement and raises the amounts of hybridized HDNA1, HDNA2, and target miRNA by SDR. However, further increases in hybridization temperature to values above 35 °C resulted in a decrease in the peak current value, which could be due to the effect of temperature on the thermodynamic properties of DNA duplex formation; this effect affects the hybridization and substitution efficiency between the DNA strands and miRNA in SDR. Consequently, the optimized hybridization temperature adopted for the biosensor was 35 °C.

3.5. Electrochemical determination of miRNA-21 by I-T

The analytical performance of the proposed biosensor, including its sensitivity, linear range, and limit of detection (LOD) were investigated

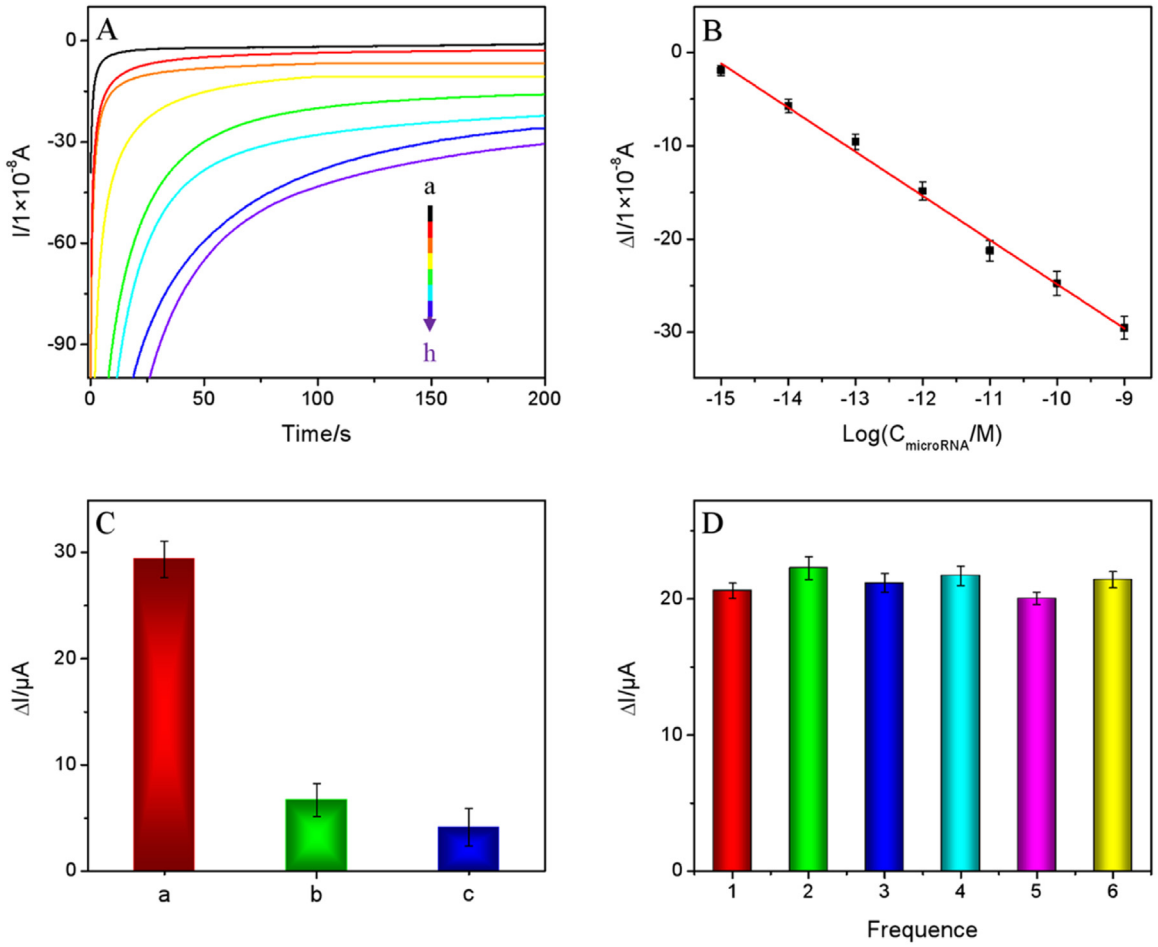

Fig. 4. I-T responses (A) to Fc-HDNA2&HDNA1/p-DNA/NCS/Mo_2C NS/GCE fabricated biosensor after capturing different concentrations of miRNA-21 from (a) to (h): 0 M, 1 fM, 10 fM, 100 fM, 1 p.M., 10 p.M., 100 p.M. and 1 nM in 0.01 M PBS (pH = 7.0). (B) Calibration curve of net peak current vs. logarithmic miRNA-21 concentration. Error bars = RSD (n = 5). (C) I-T responses of the proposed biosensor in specificity for complementary target miRNA-21 (a), single-base mismatch miRNA (b) and non-complementary miRNA (c) in 0.01 M PBS (pH = 7.0), and the concentrations were 1 nM respectively. The electrochemical I-T response of independently fabricated six biosensors (D), and the concentrations were 10 p.M. respectively. Error bars = RSD (n = 5).

Table 1
Comparison of different biosensors for determination of nucleic acids.

Method	Analyte	Method of signal amplification	Linear arrange	Detection limit	Reference
FRET	microRNA − 21	MoS_2 QDs@MBs/FAM tag/microRNA − 21	5 nM − 150 nM	0.38 nM	(Yu et al., 2018)
Electrochemical Biosensor (DPV)	microRNA − 21	AuE/capture probe/CHA/RCA/ST-AP	0.5 p.M. − 12.5 nM	0.29 p.M.	(Li et al., 2018)
QCM mass sensor	microRNA − 21	Gold-coated quarts crystals/Cp-DNA/target microRNA-AuNPs	0.1 p.M. − 50 p.M.	28 fM	(Premaratne et al., 2017)
SPR microarray	mimic	SPR gold array chip/Cp-DNA/target microRNA-AuNPs		47 fM	
Electrochemical Biosensor (SWV)	Wnt7B gene	AuE/hairpin Cp-DNA-MB/MCH/target DNA/enzymatic isothermal amplification	2 fM − 500 p.M.	1.6 fM	(Li et al., 2016a)
Amperometric/DPV	microRNA − 377	AuE/Cp-DNA/MCH/microRNA − 377/SDA/ST-AP	1.0 fM − 1.0 nM	0.68 fM	(Hu et al., 2017)
Electrochemical Biosensor (DPV)	P53 gene	AuE/capture DNA/target DNA/HCR/PANI	1.0 fM − 100 p.M.	0.5 fM	(Ding et al., 2018)
Electrochemical Biosensor (DPV)	microRNA − 21	Au-μPAD/HP/microRNA − 21/CeO_2-Au@COx/Ru$(NH_3)_6^{3+}$	1.0 fM − 1 p.M.	0.434 fM	(Sun et al., 2018)
Fluorescence	DNA	LFNAB/Cp-DNA/target DNA/FCN-DNA	1.0 fM − 10 nM	0.4 fM	(Takalkar et al., 2017)
Amperometric/I-T	microRNA − 21	GCE/NCS/Mo_2C nanosheet/p-DNA/HDNA1&HDNA2-Fc	1 fM − 1 nM	0.34 fM	This work

by measuring I–T response at 200 s to different concentrations of the target miRNA-21. Results recorded in 0.1 M PBS (pH 7.0) under the optimal conditions of the experiment are shown in Fig. 4. A control experiment without target miRNA was also carried out (Fig. 4A, curve a). From Fig. 4A, the I–T current increased (from a to h) following the increase in target miRNA-21 concentration. Fig. 4B shows excellent linearity between the net terminal currents and the logarithm of target miRNA-21 concentrations in the range of 1 fM to 1 nM. The resulting linear equation was $\Delta I = -72.2$ to $4.73\mathrm{Log}(C_{microRNA}/M)$ with a correlation coefficient of 0.9938; here, ΔI represents the terminal current subtracted from the blank response for each data point. The limit of detection was 0.34 fM (S/N = 3), which is competitive with or even superior to previously reported signal amplification strategies (Table 1). Thus, the proposed strategy of SDR via cascade displacement

amplification significantly contributes to signal amplification and improvement of detection sensitivity. This performance improvement could be attributed to several reasons: (1) Owing to the specific recognition of HDNA1, HDNA2 and miRNA for hybrids and substitute circularly activated SDR for recycling amplification, causing the assembly of numerous HDNA complexes. (2) The excellent biocompatibility and conductivity of NCS/Mo_2C NS improved the biological activity of p-DNA, which could specifically hybrid with the target-induced HDNA complex. The electrochemical signals were induced only by the target miRNA. In the absence of target miRNA, the background signal was weak, significantly reduces the background signals. Finally, (3) the spatial proximity of the redox probe Fc to the GCE is particularly advantageous in promoting the electrochemical redox efficiency of Fc.

3.6. Specificity and reproducibility of the biosensor

To verify the selectivity of the developed biosensor, HDNAs were separately hybridized with 1 nM single base mismatched target and 1 nM non-complementary oligonucleotides and subjected to I–T signal measurement. A much higher current change was detected from miRNA-21 than from 3.9 times the single base mismatched target and 5.7 times the non-complementary oligonucleotides (Fig. 4C). The developed sensor showed good specificity and ability to differentiate between the target molecule and other possible interference oligonucleotides. In Fig. 4D, the reproducibility of the biosensor was evaluated by measuring six batches of the sensor in the presence of 10 p.M. miRNA-21. The relative standard deviations (RSD) obtained were below 5.7%, which confirms the good reproducibility of the sensor.

3.7. Detection of target miRNA in real samples

A standard-addition experiment in 10-fold diluted human serum samples were carried out to explore the application potential of the proposed sensor in complex biological matrices. Serum samples spiked with different concentrations (100 fM, 1 p.M., 10 p.M., 100 p.M., and 1 nM) of chemically synthesized miRNA-21 were tested using the strategy we designed. The recovery values ranged from 92.0% to 113.1%, and the corresponding RSDs ranged from 1.17% to 5.095% for miRNA-21 (Table S2), which is in good agreement with results reported by other researchers (Su et al., 2017; Fan et al., 2017). In addition, the corresponding I–T response curves between the serum and standard samples exhibited a similar trend, as shown in Fig. S2. These results suggest that the established miRNA biosensor is a promising analytical equipment that could detect miRNA in real samples.

To investigate the feasibility of the proposed biosensor for complex biological matrix detection, we analyzed miRNA-21 in the cell lysate samples extracted from two cancerous cell lines, HeLa (cervical cancer cells, a cell line with low expression of miRNA-21) and MCF-7 (human breast cancer cell lines, a cell line with high expression of miRNA-21). As shown in Fig. S3, the lysates of Hela and MCF-7 cells were incubated on the electrochemical biosensor. With the number of Hela cells increased from 100 to 10^5 cells, only a slight increase in the current signal was observed, which suggests low miRNA-21 expression in HeLa cells. By contrast, when the biosensor was incubated with the lysates of MCF-7 cells, a dramatic increase in the current response could be observed as the cell number increased from 100 to 10^5. This phenomenon indicates that miRNA-21 is highly expressed in MCF-7 cells. These results are consistent with previous reports (Cai et al., 2017; Zhang et al., 2016, 2017). Therefore, the proposed electrochemical biosensor provides a potential assay for monitoring miRNA in cancer cells.

4. Conclusion

We developed a facile and enzyme-free method involving an SDR signal-amplification strategy combined with NCS/Mo_2C NS on electrode substrates to allowing the sensitive detection of miRNA-21 with high sensitivity and specificity. The designed NCS/Mo_2C NS exhibited great biocompatibility, good conductivity, and excellent dispersibility. SDR significantly enhanced the amount of signal molecules triggered by trace target miRNA-21 and brought the Fc close to the electrode surface, thereby improving electrochemical redox efficiency of the biosensor. Our strategy exhibited great analytical performance for breast cancer-related miRNA-21 detection with a wide detection range of 1 fM to1 nM and a relative low LOD of 0.34 fM; it also demonstrated reliable reproducibility of RSD $<$ 5.7% and the absence of false positive signals caused by non-specific adsorption and loss of signal molecules. Given the advantages of our innovative sensing strategy, the proposed biosensing platform could be extended to the in vitro early detection of various disease biomarkers in clinical and point-of-care applications.

Acknowledgements

This research was financially supported by the National Nature Science Foundations of China (No. 81571812) and A Project Funded by the Priority Academic Program Development of Jiangsu Higher Education Institutions (1107047002).

Appendix A. Supplementary material

Supplementary data associated with this article can be found in the online version at doi:10.1016/j.bios.2018.09.037.

References

Arya, S.K., Bhansali, S., 2011. Chem. Rev. 111, 6783–6809.
Azimzadeh, M., Rahaie, M., Nasirizadeh, N., Ashtari, K., Naderi-Manesh, H., 2016. Biosens. Bioelectron. 77, 99–106.
Bi, S., Yue, S.Z., Wu, Q., Ye, J.Y., 2016. Biosens. Bioelectron. 83, 281–286.
Cai, W., Xie, S.B., Tang, Y., Chai, Y.Q., Yuan, R., Zhang, J., 2017. Talanta 163, 65–71.
Chen, Z.Q., Liu, Y., Xin, C., Zhao, J.K., Liu, S.F., 2018. Biosens. Bioelectron. 113, 1–8.
Cui, H.F., Wu, W.W., Li, M.M., Song, X.J., Lv, Y.X., Zhang, T.T., 2018. Biosens. Bioelectron. 99, 223–229.
Ding, L.H., Zhang, L.N., Yang, H.M., Liu, H.Y., Ge, S.G., Yu, J.H., 2018. Sens. Actuat. B-Chem. 268, 210–216.
Dinshaw, I.J., Muniandy, S., Teh, S.J., Ibrahim, F., Leo, B.F., Thong, K.L., 2017. J. Electroanal. Chem. 806, 88–96.
Dong, H.F., Lei, J.P., Ding, L., Wen, Y.Q., Ju, H.X., Zhang, X.J., 2013. Chem. Rev. 113, 6207–6233.
Fan, T.T., Mao, Y., Liu, F., Zhang, W., Yin, J.X., Jiang, Y.Y., 2017. Sens. Actuat. B-Chem. 249, 1–7.
Feng, C., Mao, X.X., Yang, Y.C., Zhu, X.L., Yin, Y.M., Li, G.X., 2016. J. Electroanal. Chem. 781, 223–232.
Ge, S.G., Zhao, J.G., Wang, S.P., Lan, F.F., Yan, M., Yu, J.H., 2018. Biosens. Bioelectron. 102, 411–417.
Halim, J., Kota, S., Lukatskaya, M.R., Naguib, M., Zhao, M.Q., Moon, E.J., Pitock, J., Nanda, J., May, S.J., Gogotsi, Y., Barsoum, M.W., 2016. Adv. Funct. Mater. 26, 3118–3127.
Hou, T., Li, W., Liu, X.J., Li, Feng, 2015. Anal. Chem. 87, 11368–11374.
Hu, R., Wang, G.L., Yuan, R., Xu, Y.J., Yu, T.X., Zhong, L., Zhou, Q., Ding, S.J., 2017. J. Electroanal. Chem. 789, 160–166.
Jiang, J.J., Lin, X.Y., Ding, D., Diao, G.W., 2018. Biosens. Bioelectron. 114, 37–43.
Lee, J.M., Cho, H., Jung, Y., 2010. Angew. Chem. Int. Ed. 122, 8844–8847.
Li, J.L., Chen, Z.P., Xiang, Y., Zhou, L.L., Wang, T., Zhang, Z., Sun, K.X., Yin, D., Li, Y., Xie, G.M., 2016a. Biosens. Bioelectron. 86, 75–82.
Li, Q., Zeng, F.P., Lyu, N., Liang, J., 2018. Analyst 143, 2304–2309.
Li, X.L., Guo, J., Zhai, Q., Xia, J., Yi, G., 2016b. Anal. Chim. Acta 934, 52–58.
Li, X.M., Cheng, W., Li, D.D., Wu, J.L., Ding, X.J., Cheng, Q., Ding, S.J., 2016c. Biosens. Bioelectron. 80, 98–104.
Lin, Z.X., Wan, W.M., Yao, S.Y., Chen, J.G.G., 2018. Appl. Catal. B-Environ. 233, 160–166.
Lisak, G., Arnebrant, T., Lewenstam, A., Bobacka, J., Ruzgas, T., 2016. Anal. Chem. 88, 3009–3014.
Mak, W.C., Beni, V., Turner, A.P.F., 2016. TrAC-Trend Anal. Chem. 79, 297–305.
Miao, X.M., Wang, W.H., Kang, T.S., Liu, J.B., Shiu, K.K., Leung, C.H., Ma, D.L., 2016. Biosens. Bioelectron. 86, 454–458.
Nguyen, T.T., Trinh, K.T.L., Yoon, W.J., Lee, N.Y., Ju, H., 2017. Sens. Actuat. B-Chem. 242, 1–8.
Premaratne, G., Al Mubarak, Z.H., Senavirathna, L., Liu, L., Krishnan, S., 2017. Sens. Actuat. B-Chem. 253, 368–375.
Rohaizad, N., Mayorga-Martinez, C.C., Sofer, Z., Pumera, M., 2017. ACS Appl. Mater. Inter. 9, 40697–40706.
Shi, K., Dou, B.T., Yang, J.M., Yuan, R., Xiang, Y., 2017. Biosens. Bioelectron. 87, 495–500.

Sreekanth, K.V., Alapan, Y., ElKabbash, M., Ilker, E., Hinczewski, M., Gurkan, U.A., Luca, A.D., Strangi, G., 2016. Nat. Mater. 15, 621–627.
Su, S., Cao, W.F., Liu, W., Lu, Z.W., Zhu, D., Chao, J., Weng, L.X., Wang, L.H., Fan, C.H., Wang, L.H., 2017. Biosens. Bioelectron. 94, 552–559.
Sun, X.F., Wang, S.L., Zhang, Y.P., Tian, Y.P., Zhou, N.D., 2017. Sens. Actuat. B-Chem. 252, 306–312.
Sun, X.L., Wang, H., Jian, Y.N., Lan, F.F., Zhang, L.N., Liu, H.Y., Ge, S.G., Yu, J.H., 2018. Biosens. Bioelectron. 105, 218–225.
Takalkar, S., Baryeh, K., Liu, G.D., 2017. Biosens. Bioelectron. 98, 147–154.
Tian, L., Qi, J.X., Qian, K., Oderinde, O., Cai, Y.Y., Yao, C., Song, W., Wang, Y.H., 2018. Sens. Actuat. B-Chem. 260, 676–684.
Tiwari, J.N., Vij, V., Kemp, K.C., Kim, K.S., 2016. ACS Nano 10, 46–80.
Ullah, S., Hamade, F., Bubniene, U., Engblom, J., Ramanavicius, A., Ramanaviciene, A., Ruzgas, T., 2018. Biosens. Bioelectron. 110, 175–179.
Valenti, G., Scarabino, S., Goudeau, B., Lesch, A., Jovic, M., Villani, E., Sentic, M., Rapino, S., Arbault, S., Paolucci, F., Sojic, N., 2017. J. Am. Chem. Soc. 139, 16830–16837.
Várallyay, E., Burgyán, J., Havelda, Z., 2008. Nat. Protoc. 3, 190–196.
Wang, H., Jian, Y.N., Kong, Q.K., Liu, H.Y., Lan, F.F., Liang, L.L., Ge, S.G., Yu, J.H., 2018a. Sens. Actuat. B-Chem. 257, 561–569.
Wang, H., Zhou, C.X., Sun, X.L., Jian, Y.N., Kong, Q.K., Cui, K., Ge, S.G., Yu, J.H., 2018b. Biosens. Bioelectron. 117, 651–658.
Wu, C., Li, J.H., 2017. ACS Appl. Mater. Inter. 9, 41314–41322.
Xu, B.Z., Zhu, M.S., Zhang, W.C., Zhen, X., Pei, Z.X., Xue, Q., Zhi, C.Y., Shi, P., 2016. Adv. Mater. 28, 3333–3339.
Yang, D.W., Tang, Y.G., Miao, P., 2017. TrAC-Trend Anal. Chem. 94, 1–13.
Yang, Q., Gu, W.W., Gu, Y., Yan, N.N., Mao, Y.Y., Zhen, X.X., Wang, J.M., Yang, J., Shi, H.J., Zhang, X., Wang, J., 2018. J. Transl. Med. 16, 186.
Yao, J., Zhang, Z., Deng, Z.H., Wang, Y.Q., Guo, Y.C., 2017. Analyst 142, 4116–4123.
Yin, D., Tao, Y.Y., Tang, L., Li, W., Zhang, Z., Li, J.L., Xie, G.M., 2017. Microchim. Acta 184, 3721–3728.
Yu, S.L., Chen, H.Y., Chang, G.C., Chen, C.Y., Chen, H.W., Singh, S., Cheng, C.L., Yu, C.J., Lee, Y.C., Chen, H.S., Su, T.J., Chiang, C.C., Li, H.,N., Hong, Q.S., Su, H.Y., Chen, C.C., Chen, W.J., Liu, C.C., Chan, W.K., Chen, W.J., Li, K.C., Chen, J.J.W., Yang, P.C., 2008. Cancer Cell 13, 48–57.
Yu, X.S., Hu, L.Z., Zhang, F., Wang, M., Xia, Z.N., Wei, W.L., 2018. Microchim. Acta 185, 239.
Zhai, Q.F., Zhang, X.W., Li, J., Wang, E.K., 2016. Nanoscale 8, 15303–15308.
Zhang, K., Dong, H.F., Dai, W.H., Meng, X.D., Lu, H.T., Wu, T.T., Zhang, X.J., 2017. Anal. Chem. 89, 648–655.
Zhang, K., Wang, K., Zhu, X., Xie, M.H., 2016. Sens. Actuat. B-Chem. 223, 586–590.
Zhu, X.Q., Zhai, Q.F., Gu, W.L., Li, J., Wang, E.K., 2017. Anal. Chem. 89, 12108–12114.